IEEE Photonics Journal
An IEEE Photonics Society Publication

Open Access

Theoretical Investigation of Intersections of Metal-Insulator-Silicon-Insulator-Metal Waveguides

Volume 8, Number 6, December 2016

Min-Suk Kwon
Yonghan Kim

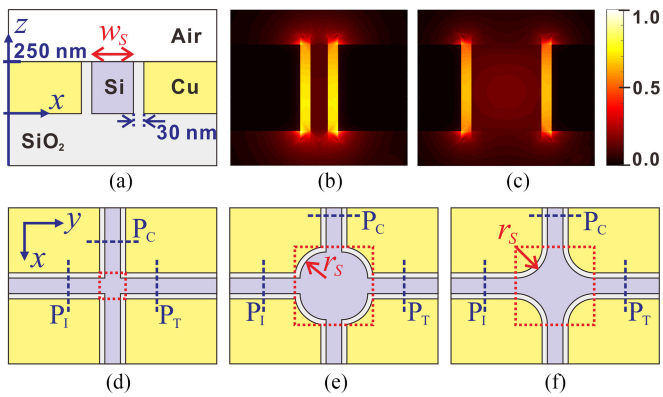

DOI: 10.1109/JPHOT.2016.2627639
1943-0655 © 2016 IEEE

IEEE photonics SOCIETY

IEEE

Theoretical Investigation of Intersections of Metal-Insulator-Silicon-Insulator-Metal Waveguides

Min-Suk Kwon and Yonghan Kim

School of Electrical and Computer Engineering, Ulsan National Institute of Science and Technology, Ulsan 689-798, South Korea

DOI:10.1109/JPHOT.2016.2627639

Manuscript received October 13, 2016; revised November 6, 2016; accepted November 8, 2016. Date of publication November 11, 2016; date of current version December 1, 2016. This work was supported by the Basic Science Research Program through the National Research Foundation of Korea funded by the Ministry of Education under Grant 2013R1A1A2A10062227. Corresponding author: M.-S. Kwon (e-mail: mskwon@unist.ac.kr).

Abstract: We theoretically investigate simple, circle-shaped, and diamond-shaped intersections of metal-insulator-silicon-insulator-metal (MISIM) waveguides. Because of the strong light confinement of the hybrid plasmonic waveguides, the simple intersection does not work efficiently. The low efficiency of the simple intersection is improved in the other intersections, and the diamond-shaped intersection is superior to the circle-shaped one. When the footprint of the diamond-shaped intersection is just 1.96 μm^2, its throughput is between –0.68 and –0.78 dB in the wavelength interval between 1.45 and 1.60 μm, and its crosstalk is smaller than –18 dB in the interval. This compact, efficient intersection may pave the way to on-chip hybrid networks of photonic and plasmonic devices.

Index Terms: Plasmonics, silicon nanophotonics, waveguides, waveguide devices.

1. Introduction

Nanoplasmonic waveguides are based on surface plasmon polaritons propagating along metal-dielectric interfaces such that they strongly confine light in a region much smaller than the diffraction limit [1]. Their strong light confinement may enable large-scale photonic integrated circuits to be realized [2]. This tangible possibility has driven a plethora of research on nanoplasmonic waveguide devices for more than a decade. For example, nanoplasmonic resonators [3], [4], polarization rotators [5], [6], and modulators [7], [8], which have footprints of the order of 1 μm^2, have been studied. However, such studies have mainly focused on development of discrete components. The next step is naturally to investigate an on-chip network of diverse nanoplasmonic waveguide devices. To do so, it is indispensable to devise efficient intersections of nanoplasmonic waveguides. Efficient intersections mean that the transmission of a through waveguide or throughput is maximized and the crosstalk into a crossing waveguide is minimized. Paradoxically, the strong light confinement hinders nanoplasmonic waveguide crossings from working efficiently.

A few nanoplasmonic intersections have been studied until now [9]–[12]. Their operation principles are very similar to those of 90° intersections of silicon photonic waveguides, which are based on resonance-assisted tunneling [13], adiabatic mode expansion [14], [15], and multimode interference (MMI) [16], [17]. For example, Xiao *et al.* reported the intersection of one-dimensional

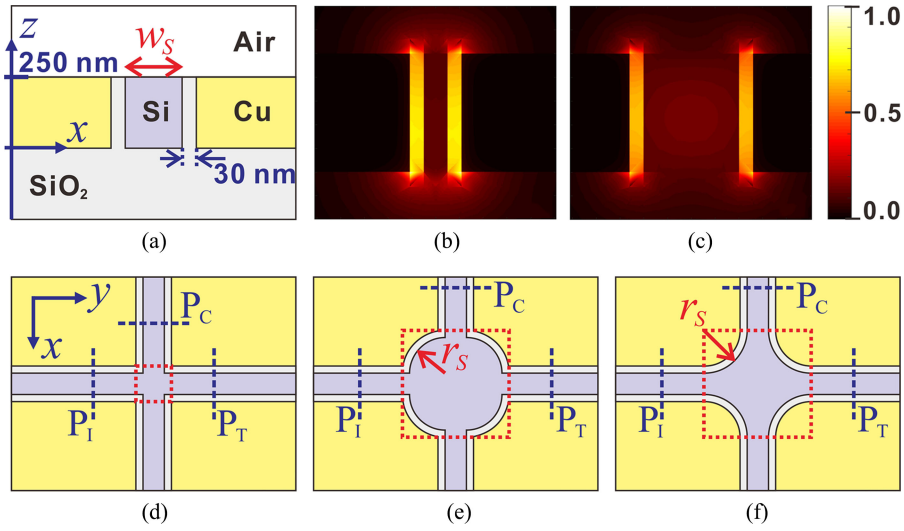

Fig. 1. (a) Cross-sectional structure of the MISIM waveguide. (b) and (c) Distributions of |**E**| of the fundamental TE mode of the MISIM waveguide for $w_S = 50$ and 200 nm. (d) to (f) Structures of the simple (d), circle-shaped (e), and diamond-shaped (f) intersections. These show the structures in the *xy*-plane at $z = 125$ nm. The input, through, and crossing ports of the intersections are at P_I, P_T, and P_C, respectively. The red dotted squares denote the actual regions of the intersections.

metal-insulator-metal waveguides, which is based on resonance-assisted tunneling [9]. The calculated throughput is –2.7 dB, although the crosstalk can be made smaller than –26 dB. Tsilipakos *et al.* reported the intersection of dielectric-loaded plasmonic waveguides [10]. In the intersection, the elliptically expanded waveguides cross. Its throughput except propagation loss is –0.8 dB, and its crosstalk is –37 dB. However, its footprint is 36 μm^2. Li *et al.* reported the intersection of conductor-gap-silicon (CGS) plasmonic waveguides [11]. Since it is based on a MMI structure, it occupies quite large area, which is 19.1 μm^2. The calculated throughput and crosstalk are –1.25 and –17.2 dB, respectively. The characteristics of the previous intersections indicate that it is still required to develop efficient, compact intersections of nanoplasmonic waveguides.

Among a large variety of nanoplasmonic waveguides [18]–[21], metal-insulator-silicon- insulator-metal (MISIM) waveguides [22]–[27], which are silicon-based hybrid plasmonic waveguides, are most likely to be an essential building block of on-chip hybrid networks of photonic and plasmonic waveguide devices. This is reasonable anticipation due to their good properties: they have been fabricated by using standard CMOS technology; they have small propagation losses; and they can be easily integrated with and efficiently coupled to silicon photonic waveguides. In this paper, therefore, intersections of MISIM waveguides are theoretically investigated. Simple, circle-shaped, and diamond-shaped intersections are analyzed and compared. The second and third intersections are basically crossings of expanded MISIM waveguides. However, resonance modes exist in the crossing regions such that they rather reduce the throughputs of the intersections around some wavelengths, which is different from the resonance-assisted tunneling. The second and third intersections improve the characteristics of the simple intersection. The comparison shows that the diamond-shaped intersection is superior to the circle-shaped intersection. The throughput of the diamond-shaped intersection reaches –0.68 dB when the intersection occupies just 1.96 μm^2. In terms of throughput and footprint, the diamond-shaped intersection is better than the previous intersections.

2. Intersection structures and analysis method

The intersections investigated in this paper consist of the MISIM waveguides which have the cross-sectional structure shown in Fig. 1(a). The MISIM waveguide comprises a 250-nm-high silicon (Si)

strip of width w_S and copper (Cu) patterns sandwiching the Si strip with 30-nm-thick silicon dioxide (SiO_2) layers in between. The structure is slightly different from that of the MISIM waveguides realized previously, but there is no significant influence of the difference on the characteristics of the intersections. The distributions of the electric field **E** of the fundamental transverse electric (TE) mode of the MISIM waveguide are shown for $w_S = 50$ nm and $w_S = 200$ nm in Fig. 1(b) and (c), respectively. The electric field is strongly confined in the narrow SiO_2 layers. As w_S increases, the confinement in the SiO_2 layers becomes weak, and the portion of the electric field confined in the Si strip increases. The intersection structures in the *xy*-plane at $z = 125$ nm are shown in Fig. 1(d) to 1(f) (the plane at $z = 125$ nm is the mid-plane cutting through the Si strip and the Cu patterns). In the simple intersection, the two MISIM waveguides simply cross. The circle-shaped intersection consists of the Si strip crossing, every corner of which has a 90° Si sector of radius r_S. The diamond-shaped intersection consists of the Si strip crossing, every corner of which has the Si pattern resulting from removing a 90° Si sector of radius r_S from a Si square of side r_S.

The finite difference time domain (FDTD) method (FDTD Solutions, Lumerical) was used to analyze the 3-D intersections based on the two-dimensional MISIM waveguide. For the analysis, the material models of Si and SiO_2 in FDTD Solutions were used; the refractive index of Cu was obtained from the multi-coefficient model based on the measured dielectric constant of Cu [28]. The refractive indices of Si, SiO_2, and Cu at the wavelength $\lambda = 1.55\,\mu$m are 3.477, 1.444, and $0.2988 - j10.8303$, respectively. The input, through, and crossing ports of the intersections are at positions P_I, P_T, and P_C, respectively, which are 500 nm away from the boundaries of the regions occupied by the intersections. The fundamental transverse-electric (TE) mode of the MISIM waveguide was launched at P_I. Then, the transmission of the MISIM waveguide mode into the through waveguide (i.e., throughput) was calculated at P_T, and that into the transverse waveguide (i.e., crosstalk) was calculated at P_C. The throughputs and the crosstalks include the loss of the MISIM waveguide of length 1 μm and the Ohmic losses of the actual intersection regions.

3. Characteristics of the three intersections

The calculated throughput and crosstalk of the simple intersection at $\lambda = 1.552\,\mu$m are shown in Fig. 2(a) for $w_S = 50$, 100, 150, and 200 nm. Overall, the throughput is small, and the crosstalk is large. Because of the strong confinement of the MISIM waveguide mode in the SiO_2 layers, the simple intersection behaves like a splitter when w_S is small. The incident MISIM waveguide mode is split and transmitted to not only the through waveguide but the crossing waveguides as well. Moreover, it is well reflected from the intersection if w_S is small. The reflectivity of the MISIM waveguide mode, which was calculated just on the left of P_I, is –5.9 dB for $w_S = 50$ nm. As w_S increases from 50 to 150 nm, the reflectivity decreases, and the throughput increases. However, the throughput for $w_S = 200$ nm is smaller than that for $w_S = 150$ nm. This difference can be explained with the throughput spectra in Fig. 2(b). Although the spectra for $w_S = 50$ and 100 nm do not change significantly with λ, those for $w_S = 150$ and 200 nm resemble resonance-related spectra, and the throughput for $w_S = 200$ nm becomes small near $\lambda = 1.6\,\mu$m. The distribution of the magnitude of the magnetic field component in the z axis, $|H_z|$ at $z = 125$ nm is shown for (w_S, λ) = (150 nm, 1.680 μm) in the inset of Fig. 2(a). The distribution confirms the splitter-like behavior of the simple intersection. Since the incident MISIM waveguide mode is reflected from the intersection, there is a sort of standing wave in the input waveguide. The distribution in the crossing waveguide is not symmetric about the central line parallel to the waveguide. This is because antisymmetric radiation modes are excited by the intersection and interfere with the MISIM waveguide mode [24]. The results in Fig. 2(a) and (b) indicate that the simple intersection is not efficient since the portion of the MISIM waveguide mode strongly confined in the SiO_2 layers is significantly transferred to the crossing waveguides.

As mentioned above, the larger w_S, the larger portion of the MISIM waveguide mode is confined in the Si strip. Therefore, the simple intersection can be improved by increasing w_S. This is confirmed from Fig. 2(c), which shows the throughput and crosstalk of the simple intersection at $\lambda = 1.552\,\mu$m for w_S between 0.7 and 1 μm, and the throughput spectra in Fig. 2(d). The throughput is increased

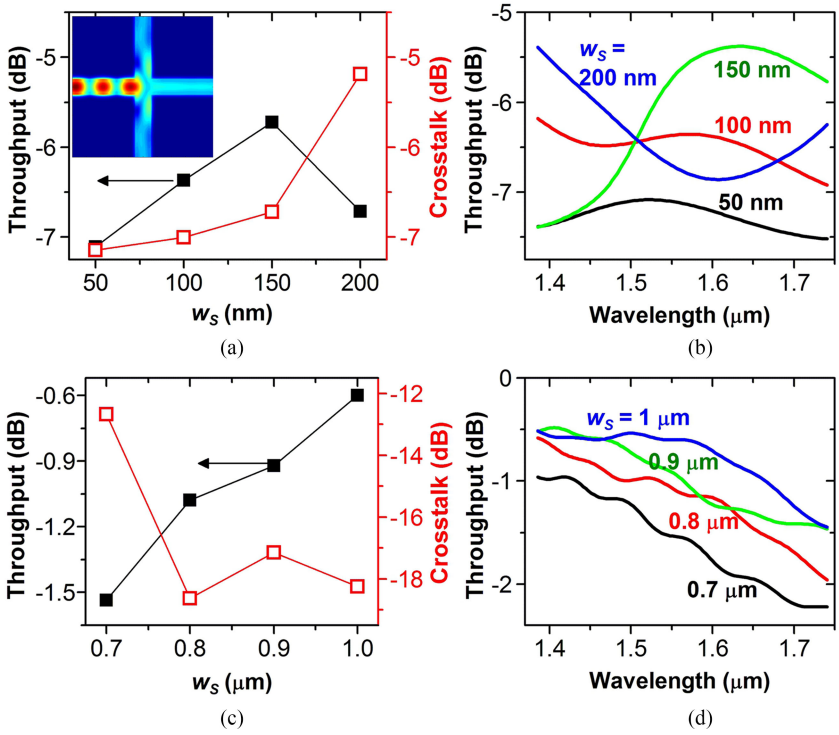

Fig. 2. Characteristics of the simple intersection. (a) Throughput and crosstalk vs. w_S. In (a), w_S = 50, 100, 150, and 200 nm. (Inset) Distribution of |Hz| at z = 125 nm for (w_S, λ) = (150 nm, 1.680 μm). (b) Throughput spectra for w_S = 50, 100, 150, and 200 nm. (c) Throughput and crosstalk vs. w_S. In (c), w_S = 0.7, 0.8, 0.9, and 1 μm. (d) Throughput spectra for w_S = 0.7, 0.8, 0.9, and 1 μm.

up to –0.6 dB, and the crosstalk is decreased down to –18 dB. However, w_S should be made small to maintain the nanoplasmonic nature, i.e., strong light confinement of the MISIM waveguides. Since Si strips wider than 193 nm guides the fundamental TE mode, the MISIM waveguides become more like photonic waveguides if $w_S >$ 193 nm. Therefore, it is necessary to expand the MISIM waveguides and make them cross. An extreme case is that the MISIM waveguides are abruptly widened and cross. Square-shaped intersections in which the individual Si strips of the MISIM waveguides are abruptly connected to a large Si square correspond to the case. They were analyzed when the MISIM waveguides have w_S = 100 nm. For example, when the side of the Si square is 700 nm, the throughput is below –5 dB, and the crosstalk is –8 dB around λ = 1.55 μm. Therefore, the MISIM waveguides should be moderately expanded. This point led us to study the circle-shaped intersection and the diamond-shaped intersection in depth.

First, the relations of the throughput and crosstalk of the circle-shaped intersection to the radius r_S, which were calculated at λ = 1.552 μm, are shown in Fig. 3(a) and (b), respectively. When r_S is smaller than 600 nm, the throughput is 3∼4 dB larger than the throughput of the simple intersection. In addition, the crosstalk of the circle-shaped intersection is 3∼4 dB smaller than that of the simple intersection. However, the throughput for r_S = 600, 800, and 900 nm becomes small, regardless of w_S. The throughput spectra for r_S = 600 nm are shown in Fig. 3(c), and those for r_S = 700 nm are shown in Fig. 3(d). When r_S = 600 nm, the spectra have the dips centered around λ = 1.55 μm. Because of these dips, the throughput for r_S = 600 nm is small. In contrast, the spectra for r_S = 700 nm have the dips centered around λ = 1.63 μm, and the throughput around λ = 1.55 μm increases. The distributions of $|H_z|$ at z = 125 nm in the intersections are shown in Fig. 3(e) and (f) for (r_S, λ) = (600 nm, 1.542 μm) and (700 nm, 1.566 μm), respectively, when w_S = 100 nm. The distribution in Fig. 3(e) is similar to that of the fifth-order resonance mode of a disk resonator [4]. As discussed below, there are resonance modes in the actual intersection

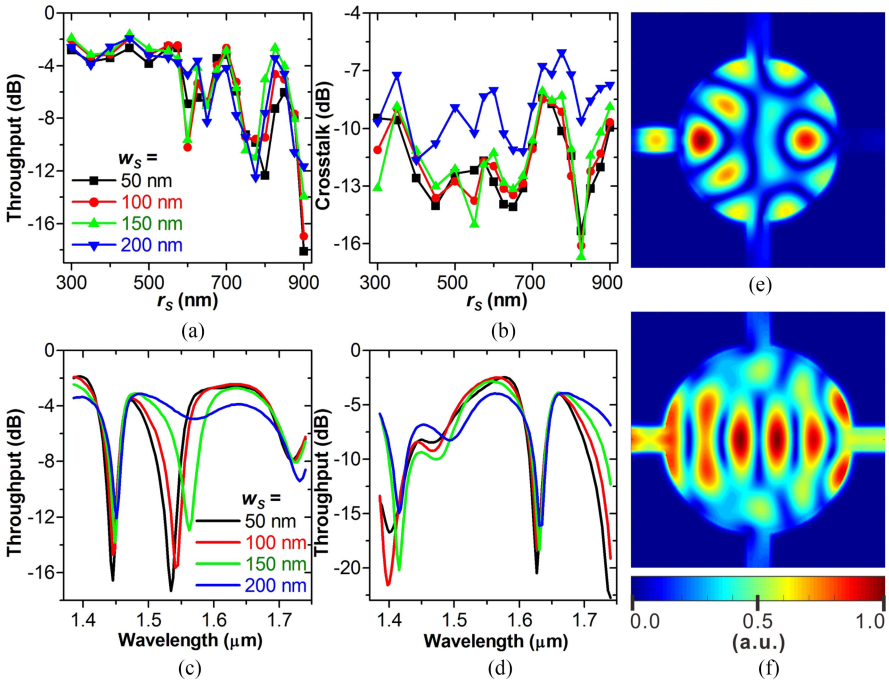

Fig. 3. Characteristics of the circle-shaped intersection. (a) Throughput vs. r_S. (b) Crosstalk vs. r_S. (c) Throughput spectra for $r_S = 600$ nm. (d) Throughput spectra for $r_S = 700$ nm. The curves in (a) to (d) are for $w_S = 50$, 100, 150, and 200 nm. (e) and (f) Distributions of $|H_z|$ at $z = 125$ nm. (e) and (f) are for (r_S, λ) = (600 nm, 1.542 μm) and (700 nm, 1.566 μm), respectively, when $w_S = 100$ nm.

region in Fig. 1(e). The incident MISIM waveguide mode is coupled to them at their resonance wavelengths and it is not transmitted but reflected, which can be checked from the standing wave pattern in the input waveguide in Fig. 3(e). This behavior of the intersection is different from that of a resonant-tunneling-assisted intersection where resonance helps its throughput increase [9], [13]. At off-resonance wavelengths, the MISIM waveguide mode is expanded and confined in the Si region of the actual intersection region and traverses the intersection as checked from Fig. 3(f). Hence, the throughput becomes large at $\lambda = 1.566\,\mu$m for $r_S = 700$ nm. The dips in the throughput spectrum red-shift as either r_S or w_S increases. The relation between the dip position and r_S or w_S is further discussed in association with Fig. 6. Although the concept of crossing the expanded MISIM waveguides makes the circle-shaped intersection better than the simple intersection, the properties of the circle-shaped intersection are not satisfactory. This is because w_S does not smoothly increase at the left and right connection positions of the actual intersection region. This problem is, to some extent, alleviated in the diamond-shaped intersection.

The relations of the throughput and crosstalk of the diamond-shaped intersection to the radius r_S, which were calculated at $\lambda = 1.552\,\mu$m, are shown in Fig. 4(a) and (b), respectively. The maximum throughput for each value of w_S is about 1 dB larger than that of the circle-shaped intersection. In addition, the minimum crosstalk for each value of w_S, which exists when the throughput is maximal, is smaller than –24 dB. Therefore, the diamond-shaped intersection is much better in quality than the circle-shaped intersection. However, the throughput still becomes small at some values of r_S, similar to that of the circle-shaped intersection. In addition, the value of r_S for which the throughput is minimal clearly decreases as w_S increases. This is different from that such a value of r_S in the case of the circle-shaped intersection weakly depends on w_S. The characteristics of the diamond-shaped intersection are quite different from those of the circle-shaped intersection. The difference between the characteristics is manifested in the throughput spectra of the diamond-shaped intersections for $r_S = 600$ and 700 nm in Fig. 4(c) and (d). In most cases, there is just one

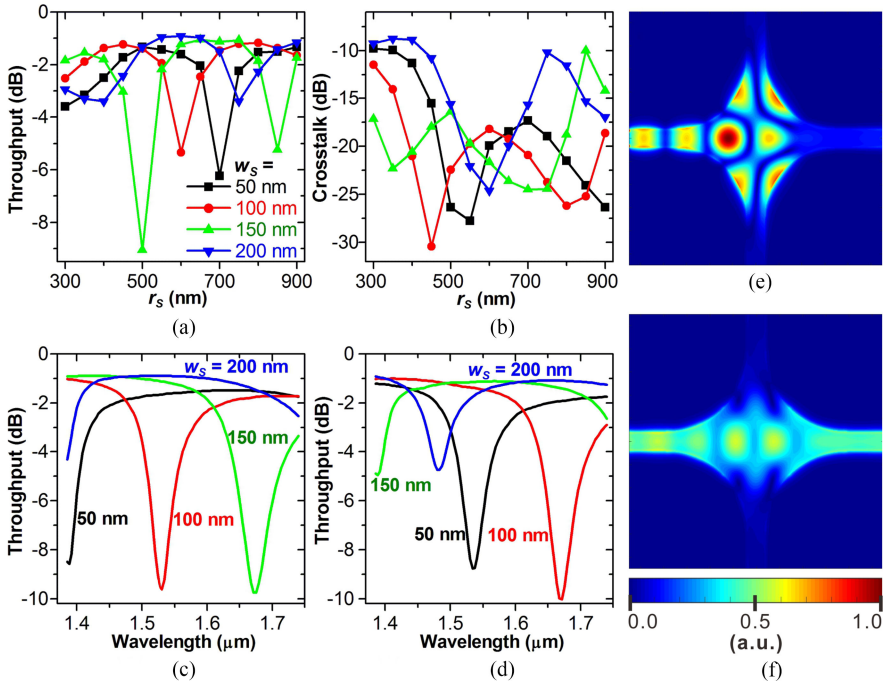

Fig. 4. Characteristics of the diamond-shaped intersection. (a) Throughput vs. r_S. (b) Crosstalk vs. r_S. (c) Throughput spectra for $r_S = 600$ nm. (d) Throughput spectra for $r_S = 700$ nm. The curves in (a) to (d) are for $w_S = 50$, 100, 150, and 200 nm. (e) and (f) Distributions of $|H_z|$ at $z = 125$ nm. (e) and (f) are for $r_S = 600$ and 700 nm, respectively, when $w_S = 100$ nm and $\lambda = 1.531\ \mu$m.

dip in the spectrum in the wavelength interval between 1.39 and 1.74 μm, and the dip significantly shifts to longer wavelengths as w_S increases. The distributions of $|H_z|$ at $z = 125$ nm in the intersections are shown in Fig. 4(e) and (f) for $r_S = 600$ and 700 nm, respectively, when $w_S = 100$ nm and $\lambda = 1.531\ \mu$m. There are resonance modes in the actual intersection region in Fig. 1(d), which are explained below, and they have properties different from those of the resonance modes related to the circle-shaped intersection. As shown in Fig. 4(e), if the incident MISIM waveguide mode is coupled to one of the resonance modes, it is not transmitted to the through waveguide but reflected. In contrast, as shown in Fig. 4(f), if one of the resonance modes is not supported by the actual intersection region, the incident MISIM waveguide mode is smoothly expanded, mainly confined in the Si region, and efficiently transmitted to the through waveguide. Consequently, the throughput approaches 1. The largest throughput around $\lambda = 1.55\ \mu$m is obtained for $w_S = 200$ nm and $r_S = 600$ nm; it is –0.9 dB. The throughput is larger than –1.0 dB in the wavelength interval between 1.45 and 1.60 μm. The minimum crosstalk is –24.6 dB, and the crosstalk is smaller than –18 dB in the interval. The crosstalk is comparable to those of the previous nanoplasmonic intersections. The reflectivity of the intersection was calculated just on the left of P_I. The reflectivity decreases from –16 to –22 dB as the wavelength increases from 1.45 to 1.60 μm. The reflectivity may be reduced by more slowly increasing and decreasing w_S (for example, if $r_S = 900$ nm, the reflectivity is below –20 dB in the wavelength interval and reaches –27 dB). If the propagation loss of the MISIM waveguide, which is 0.22 dB/μm for $w_S = 200$ nm, is considered, the throughput of only the actual intersection region is between –0.68 and –0.78 dB in the wavelength interval. Therefore, the diamond-shaped intersection operates efficiently in a broad wavelength range while it occupies a small area, which is 1.96 μm^2. The throughput is larger than those of the previous nanoplasmonic intersections [9]–[11], and the footprint is one order of magnitude smaller than those of the intersection based on adiabatic mode expansion [10] and the MMI-based intersection [11].

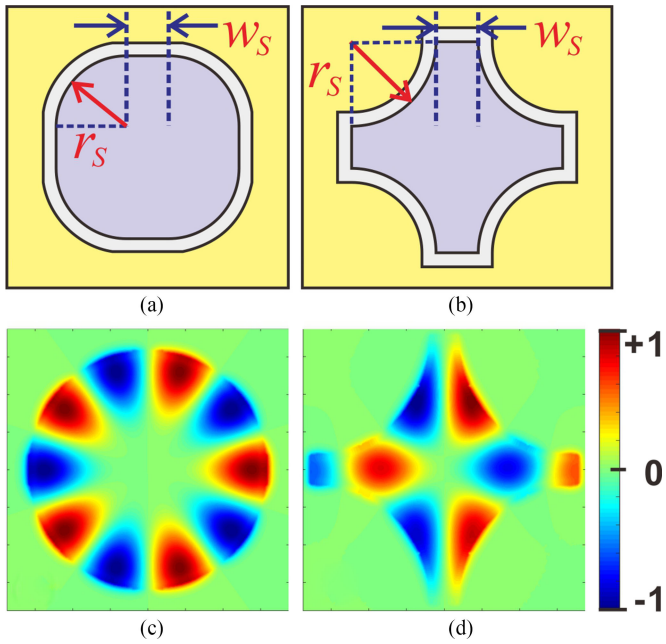

Fig. 5. Resonators associated with the actual intersection regions. (a) Structure of the circle-shaped resonator. (b) Structure of the diamond-shaped resonators. (a) and (b) Structures in the xy-plane at $z = 125$ nm. (c) Distribution of Re$[H_z]$ of the resonance mode of the circle-shaped resonator. (d) Distribution of Re$[H_z]$ of the resonance mode of the diamond-shaped resonator. (c) and (d) Distributions at $z = 125$ nm for $w_s = 100$ and $r_S = 600$ nm.

4. Discussion

The abovementioned resonance modes existing in the actual intersection regions need to be analyzed. For the analysis, the resonance modes were sought in the resonators associated with the actual intersection regions, which have the structures, respectively, shown in Fig. 5(a) and (b). The profiles of the resonance modes (i.e., distributions of the real part of H_z, Re$[H_z]$ at $z = 125$ nm) are shown in Fig. 5(c) and (d). The resonance mode in Fig. 5(c) exists in the circle-shaped resonator in Fig. 5(a) at $\lambda = 1.592\,\mu$m when $w_S = 100$ nm and $r_S = 600$ nm. The resonance mode in Fig. 5(d) exists in the diamond-shaped resonator in Fig. 5(b) at $\lambda = 1.564\,\mu$m when $w_S = 100$ and $r_S = 600$ nm. They resemble the distributions shown in Figs. 3(e) and 4(e). It is noteworthy that there is a π phase shift between the field at the left edge and the field at the right edge. When the resonance mode exists in the actual intersection region, it is likely that a part of the incident MISIM waveguide mode is coupled to the resonance mode and the remaining part is transmitted to the through waveguide. Then, the transmitted part may destructively interfere with the wave coupled from the resonance mode in the through waveguide such that the throughput becomes small.

In order to confirm the close relation between the resonance modes and the dips in the throughput spectra of the intersections, the resonance wavelengths of the former are compared with the center wavelengths of the latter in Fig. 6. As shown in Fig. 6(a), the resonance wavelengths of the circle-shaped resonator with $r_S = 600$ nm do not change significantly when w_S increases from 50 to 200 nm. This is in good agreement with that observed from the center wavelengths of the circle-shaped intersection with $r_S = 600$ nm. For $w_S = 100$ nm, Fig. 6(b) shows that the relations of the resonance wavelengths to r_S are quite similar to such relations of the center wavelengths. The resonance modes have field profiles similar to that in Fig. 5(c). If the order of the resonance mode is defined as half the number of field lobes existing along the circumference of the resonator, it is 5 or 6 in Fig. 6(a) and 4, 5, 6, or 7 in Fig. 6(b). In the case of the diamond-shaped resonator with

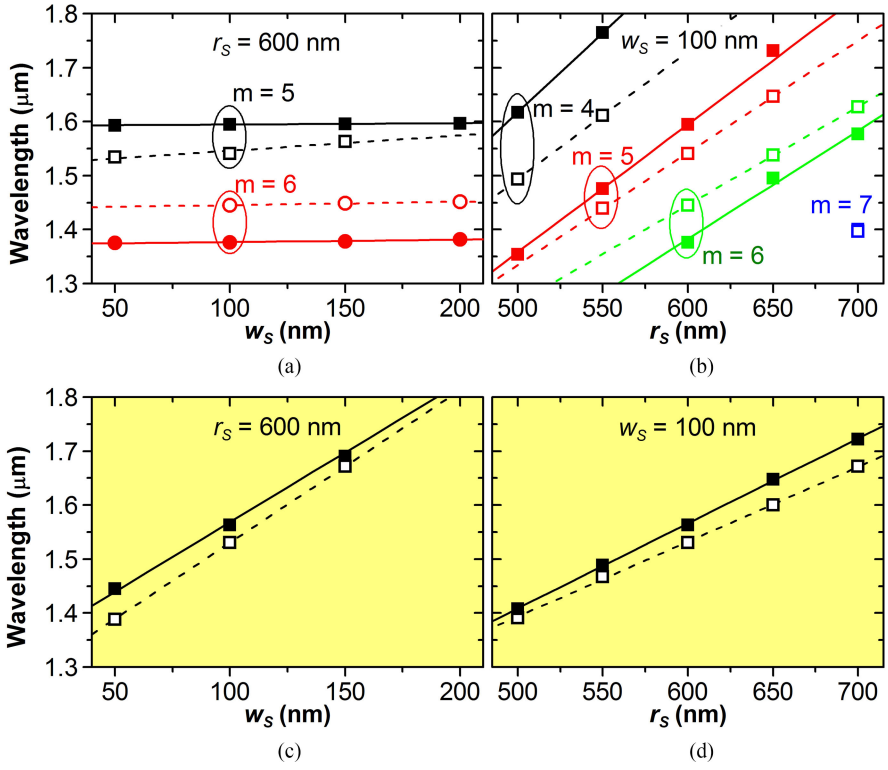

Fig. 6. Comparison between the resonance wavelengths and the center wavelengths of the dips in the throughput spectra. (a) and (b) are related to the circle-shaped resonators and intersections. (c) and (d) are related to the diamond-shaped resonators and intersections. In (a) and (c), r_S of the resonators and the intersections is set to 600 nm. In (b) and (d), w_S of the resonators and the intersections is set to 100 nm. The closed symbols represent the resonance wavelengths, and the open symbols represent the center wavelengths. The straight lines are fitted to the data.

$r_S = 600$ nm, the resonance wavelength substantially increases with w_S as shown in Fig. 6(c), which is different from the weak dependence of the resonance wavelengths on w_S in Fig. 6(a). The center wavelengths of the diamond-shaped intersection with $r_S = 600$ nm are close to the resonance wavelengths. In addition, the relation of the resonance wavelength to r_S for $w_S = 100$ nm shows good agreement with such a relation of the center wavelength in Fig. 6(d). The resonance modes related to Fig. 6(c) and (d) have almost the same field profile as that in Fig. 5(d). The results in Fig. 6 indicate that the dips in the throughput spectra are attributed to the resonance modes.

In the aforementioned analysis, the insulator thickness is fixed to 30 nm. The smaller the insulator thickness is, the more strongly the electric field of the MISIM waveguide mode is enhanced in the insulator for a fixed value of w_S. Therefore, the characteristics of the diamond-shaped intersection may depend on the insulator thickness. To check the dependence, the characteristics of the diamond-shaped intersection with $w_S = 200$ nm and $r_S = 600$ nm were calculated for the thickness of 25, 35, or 40 nm. If the thickness is 25 (40) nm, the throughput decreases by 0.092 (0.06) dB at $\lambda = 1.552\,\mu$m, and the crosstalk increases by 5.5 (1.4) dB. However, when the thickness is 35 nm, the throughput increases by 0.02 dB at $\lambda = 1.552\,\mu$m, and the crosstalk decreases by 2.1 dB. Therefore, the thickness increase of 5 nm slightly improves the characteristics of the diamond-shaped intersection.

Finally, it is intriguing to check whether the diamond-shaped intersection scheme can be applied to other plasmonic waveguides. For this purpose, the MIM waveguide which is the 100-nm-wide, 250-nm-high metal (Cu) slot embedded in SiO_2 was considered. The structure of the diamond-shaped intersection of the MIM waveguides is that in Fig. 1(d) with Si substituted with SiO_2. However,

the intersection of the MIM waveguides does not behave like that of the MISIM waveguides. As the radius of the intersection corners increases from 300 to 900 nm, the throughput decreases from –7 to –10 dB, and the crosstalk changes around –9.5 dB. Moreover, the throughput spectra slightly change with the wavelength and have no clear resonance-related dip. In addition to the diamond-shaped intersection of the MIM waveguides, that of the CGS plasmonic waveguides was also analyzed. The CGS plasmonic waveguide consists of a 220-nm-thick Si strip on a SiO_2 substrate, a 30-nm-thick SiO_2 strip on the Si strip, and a 100-nm-thick Cu strip on the SiO_2 strip. The width of the stack of the three strips is 250 nm, and the stack is covered by air. The top view of this intersection is the same as the Si pattern of the structure in Fig. 1(d). The intersection was analyzed while the radius of the intersection corners was set to 500, 600, and 700 nm. The throughput spectrum of this intersection is similar to that of the diamond-shaped intersection of the MISIM waveguides. When the radius is 700 nm, the throughput is large (around $\lambda = 1.55\,\mu$m), and the maximum is –1.5 dB at $\lambda = 1.56\,\mu$m. The crosstalk at $\lambda = 1.56\,\mu$m is –18 dB. Although the diamond-shaped intersection scheme works to some extent for the CGS plasmonic waveguides, it seems most suitable for the MISIM waveguides.

5. Conclusion

In summary, the three intersections of the MISIM waveguides have been theoretically investigated. The investigation demonstrates that the simple intersection is not efficient due to the strong light confinement of the MISIM waveguide. The diamond-shaped intersection is efficient and superior to the circle-shaped intersection. The maximum throughput of the diamond-shaped intersection reaches –0.68 dB, and its minimum crosstalk is –24.6 dB, although the area occupied by the intersection is just 1.96 μm^2. In addition, it operates well in a wide wavelength range. The diamond-shaped intersection may play a key role in implementing an on-chip hybrid network of silicon photonic waveguide devices and MISIM waveguide devices.

References

[1] D. K. Gramotnev and S. I. Bozhevolnyi, "Plasmonics beyond the diffraction limit," *Nature Photon.*, vol. 4, no. 2, pp. 83–91, Feb. 2010.
[2] M. L. Brongersma and V. M. Shalaev, "The case for plasmonics," *Science*, vol. 328, no. 5977, pp. 440–441, Apr. 2010.
[3] S. Zhu, G. Q. Lo, and D. L. Kwong, "Submicron-radius plasmonic racetrack resonators in metal-dielectric-Si hybrid plasmonic waveguides," *IEEE Photon. Technol. Lett.*, vol. 26, no. 8, pp. 833–836, Apr. 2014.
[4] M.-S. Kwon, B. Ku, and Y. Kim, "Plasmofluidic disk resonators," *Sci. Rep.*, vol. 6, pp. 23149-1–23149-8, Mar. 2016. doi: 10.1038/srep23149.
[5] J. N. Caspers, J. S. Aitchison, and M. Mojahedi, "Experimental demonstration of an integrated hybrid plasmonic polarization rotator," *Opt. Lett.*, vol. 38, no. 20, pp. 4054–4057, Oct. 2013.
[6] L. Gao *et al.*, "On-chip plasmonic waveguide optical waveplate," *Sci. Rep.*, vol. 5, 2015, Art. no. 15794. doi: 10.1038/srep15794..
[7] K. Liu, C. R. Ye, S. Khan, and V. J. Sorger, "Review and perspective on ultrafast wavelength-size electro-optic modulators," *Laser Photon. Rev.*, vol. 9, no. 2, pp. 172–194, Mar. 2015.
[8] C. Haffner *et al.*, "All-plasmonic Mach-Zehnder modulator enabling optical high-speed communication at the microscale," *Nature Photon.*, vol.9, no. 8, pp. 525–528, Aug. 2015.
[9] S. Xiao and N. A. Mortensen, "Resonant-tunneling-assisted crossing for subwavelength plasmonic slot waveguides," *Opt. Exp.*, vol. 16, no. 19, pp. 14997–15005, Sep. 2008.
[10] O. Tsilipakos, E. E. Kriezis, and S. I. Bozhevolnyi, "Thermo-optic microring resonator switching elements made of dielectric-loaded plasmonic waveguides," *J. Appl. Phys.*, vol. 109, no. 7, pp. 073111-1–073111-9, Apr. 2011.
[11] Y. Li *et al.*, "Hybrid plasmonic waveguide crossing based on the multimode interference effect," *Opt. Commun.*, vol. 335, pp. 86–89, Jan. 2015.
[12] Y. Nagasaki, M. Miyata, and M. Higuchi, "Surface plasmon propagation on overcrossing metallic waveguides fabricated by a pick-and-place method," *MRS Commun.*, vol. 5, no. 4, pp. 587–591, Dec. 2015.
[13] S. G. Johnson, C. Manolatou, S. Fan, P. R. Villeneuve, J. D. Joannopoulos, and H. A. Haus, "Elimination of cross talk in waveguide intersections," *Opt. Lett.*, vol. 23, 1855–1857 1998.
[14] W. Bogaerts, P. Dumon, D. V. Thourhout, and R. Baets, "Low-loss, low-cross-talk crossings for silicon-on-insulator nanophotonic waveguides," *Opt. Lett.*, vol. 32, no. 19, pp. 2801–2803, Sep. 2007.
[15] P. Sanchis *et al.*, "Highly efficient crossing structure for silicon-on-insulator waveguides," *Opt. Lett.*, vol. 34, no. 18, pp. 2760–2762, Sep. 2009.

[16] H. Chen and A. W. Poon, "Low-loss multimode-interference-based crossings for silicon wire waveguides," *IEEE Photon. Technol. Lett.*, vol. 18, no. 21, pp. 2260–2262, Nov. 2006.
[17] X. Li, H. Xu, X. Xiao, Z. Li, J. Yu, and Y. Yu, "Demonstration of a highly efficient multimode interference based silicon waveguide crossing," *Opt. Commun.*, vol. 312, pp. 148–152, Feb. 2014.
[18] Z. Han *et al.*, "On-chip detection of radiation guided by dielectric-loaded plasmonic waveguides," *Nano Lett.*, vol. 15, no. 1, pp. 476–480, Jan. 2015.
[19] S. J. P. Kress *et al.*, "Wedge waveguides and resonators for quantum plasmonics," *Nano Lett.*, vol. 15, no. 9, pp. 6267–6275, Sep. 2015.
[20] D. Yu. Fedyanin, D. I. Yakubovsky, R. V. Kirtaev, and V. S. Volkov, "Ultralow-loss CMOS copper plasmonic waveguides," *Nano Lett.*, vol. 16, no. 1, pp. 362–366, Jan. 2016.
[21] M. P. Nielsen *et al.*, "Adiabatic nanofocusing in hybrid gap plasmon waveguides on the silicon-on-insulator platform," *Nano Lett.*, vol.16, no. 2, pp. 1410–1414, Feb. 2016.
[22] S. Zhu, T. Y. Liow, G. Q. Lo, and D. L. Kwong, "Silicon-based horizontal nanoplasmonic slot waveguides for on-chip integration," *Opt. Exp.*, vol. 19, no. 9, pp. 8888–8902, Apr. 2011.
[23] M.-S. Kwon, J.-S. Shin, S.-Y. Shin, and W.-G. Lee, "Characterizations of realized metal-insulator-silicon-insulator-metal waveguides and nanochannel fabrication via insulator removal," *Opt. Exp.*, vol. 20, no. 20, pp. 21875–21887, Sep. 2012.
[24] J.-S. Shin, M.-S. Kwon, C.-H. Lee, and S.-Y. Shin, "Investigation and improvement of 90° direct bends of metal-insulator-silicon-insulator-metal waveguides," *IEEE Photon. J.*, vol. 5, no. 5, pp. 6601909-1–6601909-9, Oct. 2013.
[25] M. P. Nielsen, A. Ashfar, K. Cadien, and A. Y. Elezzabi, "Plasmonic materials for metal-insulator-semiconductor-insulator-metal nanoplasmonic waveguides on silicon-on-insulator platform," *Opt. Mater.*, vol. 36, no. 2, pp. 294–296, Dec. 2013.
[26] B. Ku, J.-S. Shin, and M.-S. Kwon, "Experimental investigation of plasmofluidic waveguides," *Appl. Phys. Lett.*, vol. 107, no. 20, pp. 201104-1–201104-5, Nov. 2015.
[27] X. Sun, D. Dai, L. Thylen, and L. Wosinski, "High-sensitivity liquid refractive-index sensor based on a Mach-Zehnder interferometer with a double-slot hybrid plasmonic waveguide," *Opt. Exp.*, vol. 23, no. 20, pp. 25688–25699, Sep. 2015.
[28] H. S. Lee, C. Awada, S. Boutami, F. Charra, L. Douillard, and R. E. de Lamaestre, "Loss mechanisms of surface plasmon polaritons propagating on a smooth polycrystalline Cu surface," *Opt. Exp.*, vol. 20, no. 8, pp. 8974–8981, Apr. 2012.